Periodica Polytechnica Mechanical Engineering, 69(2), pp. 182–191, 2025

Regression Analysis and Neural Network Model of Working Diameter of Ball-end Mill

Abdul Whab Mgherony[1], Balázs Mikó[1*]

[1] Institute of Mechanical Engineering and Technology, Óbuda University, Népszínház u. 8., H-1081 Budapest, Hungary
[*] Corresponding author, e-mail: miko.balazs@bgk.uni-obuda.hu

Received: 17 April 2025, Accepted: 26 May 2025, Published online: 02 June 2025

Abstract

In ball-end milling, a clear distinction exists between the nominal and the working (or effective) diameters, particularly when machining free-form surfaces. The working diameter is not constant; instead, it changes dynamically based on several factors, including the surface inclination (A_{N2}), tool diameter (D), depth of cut (a_p), and feed direction (A_f). Accurately predicting the working diameter is essential for improving surface quality and dimensional accuracy. Three primary approaches are commonly used for this purpose: the geometric model, which analytically describes the geometric relationships between machining parameters and the working diameter; regression analysis, which builds mathematical models from empirical data; and artificial neural network (ANN) models, which are capable of modeling complex, non-linear interactions between multiple input variables and the working diameter. In this study, one geometric model, two types of regression models, and two ANN models were developed and evaluated. Their performance was assessed using a set of statistical measures, including the standard deviation of the prediction error, the coefficient of determination (R^2), the root mean square error (RMSE), and the mean absolute percentage error (MAPE). These metrics provided a comprehensive basis for comparing the accuracy and reliability of each approach. The results highlight the strengths and limitations of each method in capturing the variability of the working diameter during ball-end milling of free-form surfaces.

Keywords

ball-end milling, free-form surface machining, working tool diameter, artificial neural network, regression model

1 Introduction

The adoption of freeform surfaces has seen a surge across diverse industries, encompassing aerospace, automotive, consumer products, and die and mold manufacturing. The primary tool employed for machining such surfaces, especially for finishing and pre-finishing, is the ball-end cutter. However, when using a 3-axis milling machine, distinctions arise between the nominal and working (or effective) diameter of the ball-end cutter. This discrepancy is influenced by various parameters, including cutting parameters, workpiece inclination, and cutting strategy. Consequently, determining the working diameter that aligns with the process parameters crucially influences the attainment of the desired product quality.

In the realm of the manufacturing process, engineers grapple with two primary practical challenges. The initial challenge involves determining the values of process parameters that guarantee the desired product quality, aligning with technical specifications. The second challenge revolves around the optimization of manufacturing system performance, ensuring efficient resource utilization. In this context, researchers typically strive to create a model for the machining process, a mathematical equation illustrating the relationship between process parameters (decision variables) and machining performance (responses). Essentially, models fall into three categories: geometric models, analytical models, and artificial intelligent (AI) based models.

In the context of manufacturing industry, a geometric models can be developed by emphasizing one or more aspects of machining theory, such as cutting tool properties, process kinematics, and chip formation. Computer-aided design (CAD) methods are used to build the model that simulates the machined surface profile formation. Lotfi et al. [1] utilized this approach to compute cutting forces by determining the precise engagement region and instantaneous undeformed chip thickness. Similarly, Forootan

Cite this article as: Mgherony, A. W., Mikó, B. "Regression Analysis and Neural Network Model of Working Diameter of Ball-end Mill", Periodica Polytechnica Mechanical Engineering, 69(2), pp. 182–191, 2025. https://doi.org/10.3311/PPme.40747

et al. [2] introduced a model to calculate the cutter-workpiece engagement area and cutting forces for a ball-end tool. Feng and Su [3] proposed a model for calculating instantaneous cutting forces, incorporating static cutting system deflection feedback in 3D ball-end milling. Ko and Cho [4] utilized instantaneous cutting force parameters to develop a model for forces in ball-end cutter applications. Ghorbani and Movahhedy [5] presented a model for calculating cutter-workpiece engagement boundaries in ball-end milling. In their study, Wei et al. [6] introduced a cutting force prediction approach for 3-axis ball-end milling of sculptured surfaces with Z-level contouring tool paths. To address challenges in sculptured surface machining, Wei et al. [7] presented a unique method for predicting cutting forces in three-axis ball-end milling. Nishida et al. [8] introduced a distinctive approach to calculating uncut chip thickness, utilizing a voxel model to describe both the workpiece and cutting edge. In the realm of predicting working diameter, Mikó and Zentay [9] presented a geometric model, later simulated using MATLAB by Mgherony and Mikó [10].

Analytical models, utilizing conventional approaches like the regression technique, have been applied innovatively in various studies. Cheng et al. [11] employed this approach to develop a new model predicting surface residual stress. In a similar vein, Lu et al. [12] utilized a Gaussian process regression model for accurate prediction of Ra surface roughness in compacted graphite cast iron. Addressing the intricacies of three and five-axis ball-end milling, Xu et al. [13] introduced a model to develop surface topography. This innovative model incorporates a discrete sweeping surface of the cutting edge, integrating time-varying feed speed profiles, thereby overcoming limitations in existing models. Denkena et al. [14] applied this method in their study, introducing a simulation approach that combines material removal simulation (MRS) and an empirical model to predict post-milling surface topography. Furthermore, Wojciechowski [15] contributed to this field by presenting a refined cutting force model specifically tailored to finish ball-end milling. This model factors in various elements such as cutting conditions, surface inclination (A_{N2}) angle, and cutter runout.

AI-based models, incorporating non-conventional techniques like artificial neural network (ANN), have been instrumental in various studies. Santhakumar and Iqbal [16] employed a neural network to develop a model, focusing on predicting surface roughness, specific cutting energy, and temperature during end milling operations with the trochoid toolpath strategy for AISI D3 steel. Concurrently, Lin et al. [17] introduced a model for surface roughness in end milling, taking into account cutting parameters and machining vibration. Xie et al. [18] presented an ANN-based model for spindle speed power. Proposing an intelligent prediction model, Kannadasan et al. [19] utilized the ANFIS model to predict performance indexes like average surface roughness and geometric tolerances in milled products. Additionally, Shankar et al. [20] employed artificial intelligence to forecast the wear of the cutting tool during milling processes.

In this paper, the objective is to underscore the significance of the working diameter. This is achieved through the application of both a regression model and an ANN to predict the working diameter during milling operations with a ball-end cutter.

The effective or working diameter of a ball-end milling cutter has great effect on the cutting speed, because in case of free form surface milling it will change. The changing cutting speed has effect on the chip removal process, the chip formation and the surface quality [21, 22].

The working diameter depends on the tool diameter (D), the depth of cut (a_p), the feed direction (A_f) and the inclination of the surface, which can be described by the angular position of the surface normal vector ($\boldsymbol{N}$) (A_{N1}, A_{N2}). Actually, the A_{N1} can be eliminated, if the A_f is a relative parameter. The relative A_f shows the value to the A_{N1} angle (Fig. 1). In the analysis, this relative A_f is applied.

2 Method

For a more in depth analysis of the effective diameter, it is essential to establish a mathematical model that describes effective diameter concerning cutting parameters. Two different methods were compared, the regression modelling and the ANN.

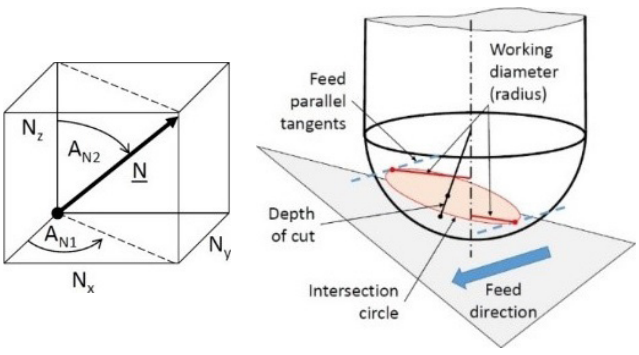

Fig. 1 Orientation of the surface normal vector and the interpretation of the tool working diameter

The base of the analysis is the set of data, which was generated by the geometry-based algorithm. In this study, the working diameter values for the ball-end tool were not based on a specific free-form surface, but were determined over the full range of possible values of A_{N2} and milling direction.

The D and the a_p were varied on 4 levels, the A_{N2}, and the relative A_f on 13 levels, as the Table 1 shows. The full factorial plan was used, because of the fast and easy calculation of the working diameter, so 2704 data were generated ($4 \times 4 \times 13 \times 13 = 2704$).

The statistical analysis of the data and the regression analysis were performed by MiniTab, (v14) [23] and Excel [24]. The neural network model was created by MATLAB [25].

The regression model and the ANN model were compared based on statistical parameters. The coefficient of determination (R^2) is the percentage of variation in the response that the model explains. The R^2 is between 0 and 1, the higher R^2 value indicates the better model:

$$R^2 = 1 - \left(\frac{\sum_{i=1}^{n} (x_i - \hat{x}_i)^2}{\sum_{i=1}^{n} (x_i - \bar{x})^2} \right), \tag{1}$$

where:

- x_i: original (measured) value;
- $\hat{x}_i$: estimated value;
- $\bar{x}$: mean value of x_i;
- n: number of data.

Root means square error (RMSE) measures the accuracy of the regression model also. The RMSE is the root square of the average value of the square of the difference of the original and estimated values.

$$\mathrm{RMSE} = \sqrt{\frac{1}{n} \times \sum_{i=1}^{n} (x_i - \hat{x}_i)^2} \tag{2}$$

Mean absolute percentage error (MAPE) means the average of the absolute value of the relative difference of the original and estimated values.

Table 1 Set of input parameters

Parameter	Values						
D	6	8	10	12	–	–	–
a_p	0.15	0.25	0.35	0.45	–	–	–
A_{N2}	40	30	20	15	10	5	1
	−5	−10	−15	−20	−30	−40	–
A_f	89	74	61	44	31	14	1
	−14	−31	−44	−61	−74	−89	–

$$\mathrm{MAPE} = \frac{1}{n} \times \sum_{i=1}^{n} \left| \frac{x_i - \hat{x}_i}{x_i} \right| \tag{3}$$

3 Results

3.1 The regression model

The main effect plots (Fig. 2) show the importance of each input parameters on the output parameter. The graphs show the mean values for each factor level connected by line.

The A_{N2} has the largest effect on the working diameter as the Fig. 2 shows. In case of the shallow section, this effect is smaller, but at the steep region, the working diameter is larger, and the relationship is not linear. The diameter of the tool and the ap have an increasing and linear effect on the working diameter. The smallest effect can be seen in case of the A_f.

The interaction plot shows (Fig. 3) how the relationship between one factor and the continuous response depends on the value of the second factor. This plot displays the average of one factor level on the x-axis, and a separate row for each level of another factor. If the lines of the diagram are parallel, there is no interaction between the factors. If the

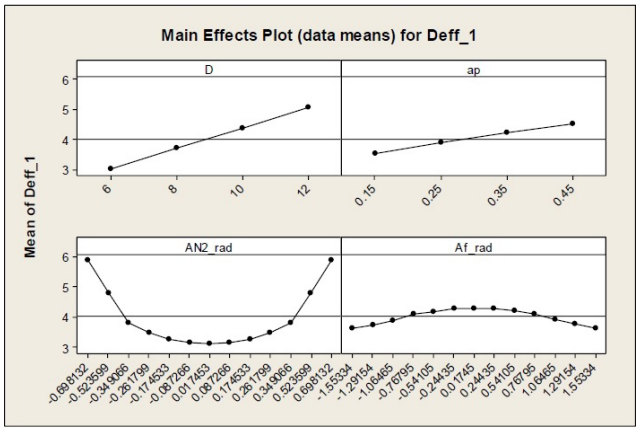

Fig. 2 The main effect plot

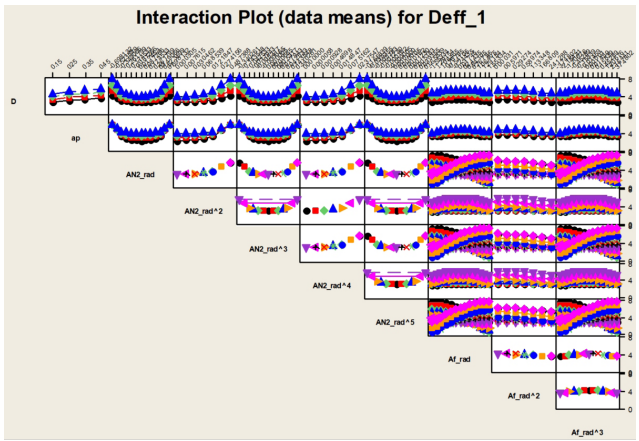

Fig. 3 Interaction plot

lines are not parallel, an interaction occurs and in this case, the multiplication of the factors must also be included in the model. Based on this, the following multipliers should also be considered in the regression model: $A_{N2} \times A_f$, $A_{N2} \times A_f^3$, $A_{N2}^3 \times A_f$, $A_{N2}^3 \times A_f^3$, $A_{N2}^5 \times A_f$, $A_{N2}^5 \times A_f^3$.

Based on the main effects plot, the interaction plot and iterations, the following equation was defined (marked as *r*1 model):

$$\begin{aligned} D_{eff} &= C + c_1 \times D + c_2 \times a_p + c_3 \times A_{N2}^2 \\ &+ c_4 \times A_{N2}^4 + c_5 \times A_f^2 + c_6 \times A_{N2} \times A_f \\ &+ c_7 \times A_{N2} \times A_f^3 + c_8 \times A_{N2}^3 \times A_f \\ &+ c_9 \times A_{N2}^3 \times A_f^3 + c_{10} \times A_{N2}^5 \times A_f + c_{11} \times A_{N2}^5 \times A_f^3. \end{aligned} \tag{4}$$

Table 2 shows the value of the coefficients of the *r*1 model. The value of the $R^2(adj)$ parameter is 91.8%.

In case of the two values of the working diameter $\left(D_{eff_1} \text{ and } D_{eff_2}\right)$ the regression model is the same, only the value of the coefficients is different.

In order to improve the accuracy of the regression model, four separate equations were created for the different *D* (marked as *r*2 model). The structure of the regression equation was the same. Table 2 shows the values of the coefficients.

The accuracy of the regression is improved, the values of the $R^2(adj)$ parameter are up to 95% in every case. However, the result is better, but instead of one equation, four equations should be used, and the *D* is not taken into account. The advised solution is to use a linear function of the *D* instead of constant coefficients. As Table 3 presents, the coefficients show linear regression in function of the *D* with good accuracy, so the separated equations could be unified in Eq. (5):

$$D_{eff} = \sum f_i(D) \times C_i. \tag{5}$$

Table 2 The coefficients of the *r*1 model

Predictor	Coefficients	*P*
C	−0.696340	0.000
c_1	0.341616	0.000
c_2	3.289690	0.000
c_3	6.548300	0.000
c_4	−1.605500	0.001
c_5	−0.282260	0.000
c_6	7.777700	0.000
c_7	−0.741100	0.000
c_8	−19.90000	0.000
c_9	3.456000	0.007
c_{10}	18.542000	0.000
c_{11}	−4.363000	0.039

3.2 The ANN model

Another way of the mathematical modelling is the use of ANN. The ANN is a multi-layered structure comprising one or more hidden layers positioned between the input and output layers. Each of these layers consist of numerous processing units called neurons, which are interconnected with adjustable weights. Within the network, every neuron receives input from all the neurons in the previous layer [21], and this is calculated as follows:

$$net_j = \sum_{j=0}^{N} w_{ij} \times x_i, \tag{6}$$

where:

- net_j: the total or net input,
- N: the number of inputs to the j^{th} neuron in the hidden layer,
- w_{ij}: the weight of the connection from the i^{th} neuron in the forward layer to the j^{th} neuron in the hidden layer,
- x_i: the input from the i^{th} neuron in the preceding layer.

Each neuron in the network generates its output (out_j) by processing the net input through an activation (transfer) function. In this study, the logistic sigmoid transfer function (also known as the sigmoid or logistic function) was used for hidden layers and a linear transfer function for the output layer in a regression task [22].

The logistic sigmoid transfer function [26, 27], often used in ANNs, is defined by Eq. (7):

$$f(x) = \frac{1}{1 + e^{-x}}, \tag{7}$$

where:

- x: the input to the function,
- e: the base of the natural logarithm (Euler's number), approximately equal to 2.71828.

The logistic sigmoid function maps any real-valued number x to an output in the range (0, 1), which makes it suitable for problems where you need to model probabilities or when you want to introduce non-linearity in the neural network.

The sigmoid function's characteristic S-shaped curve is typically used in the hidden layers of feedforward neural networks for tasks like classification. It helps transform the weighted sum of inputs into a range where the network can learn complex relationships between features.

For this study, we have designed an optimal neural network architecture using the MATLAB Neural Network

Table 3 The coefficients in *r*2 regression model for D_{eff_1}

C_i	$D = 6$	$D = 8$	$D = 10$	$D = 12$	f_i (D)	$R^2(adj)$
C	1.885	2.234	2.549	2.845	0.160D + 0.941	99.87
a_p	2.893	3.210	3.442	3.614	0.120D + 2.212	98.17
A_{N2}^2	2.634	4.982	7.762	10.815	1.366D − 5.747	99.66
A_{N2}^4	0.616	−0.461	−2.204	−4.374	−0.836D + 5.915	97.89
A_f^2	−0.218	−0.265	−0.305	−0.341	−0.020D − 0.099	99.62
$A_{N2} \times A_f$	5.258	6.987	8.643	10.223	0.828D + 0.330	99.96
$A_{N2} \times A_f^3$	−0.652	−0.717	−0.772	−0.823	−0.028D − 0.486	99.70
$A_{N2}^3 \times A_f$	−12.006	−17.176	−22.481	−27.936	−2.655D + 3.993	99.99
$A_{N2}^3 \times A_f^3$	3.665	3.628	3.368	3.163	−0.088D + 4.251	93.46
$A_{N2}^5 \times A_f$	10.410	15.600	21.105	27.052	2.772D − 6.404	99.91
$A_{N2}^5 \times A_f^3$	−4.834	−4.736	−4.173	−3.709	0.197D − 6.135	94.01
$R^2(adj)$	95.7	96.3	96.8	97.1	–	–

Toolbox [28]. In the first case (marked as *a*1 model) the network architecture comprises one input layer, one hidden layer, and one output layer. 10 neurons can be found in the hidden layer, while the input layer has four neurons, and the output layer contains two neurons during both the training and testing phases. The input layer neurons correspond with the D, the a_p, the A_{N2} and the relative A_f, while the output layer represents effective diameter $\left(D_{eff_1} \text{ and } D_{eff_2}\right)$. While in the second case (marked as *a*2 model) the network has two hidden layers: 10 neurons in the first hidden layer, and 5 in the second hidden layer.

In Figs. 4 and 5, it's evident that more than 1000 samples, in addition to approximately 400 validation and test samples, exhibit an error of 0.01034 in the context of a neural network configuration with a single hidden layer. On the contrary, when employing a model with two hidden layers, approximately 1200 samples and 400 validation and test samples display a notably reduced error of

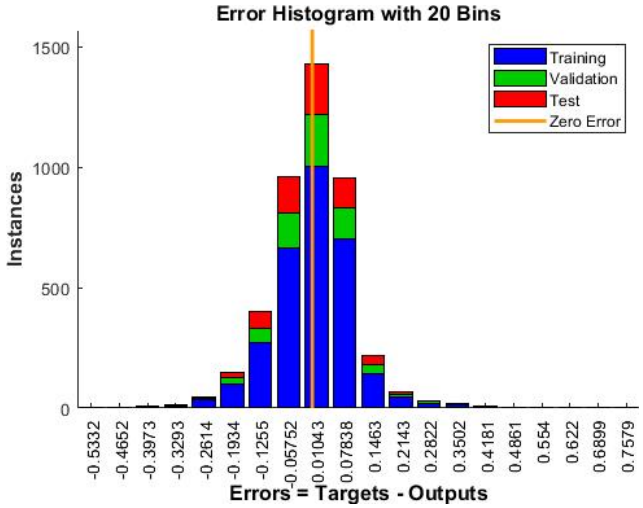

Fig. 4 Histogram error in the case of 1 hidden layer

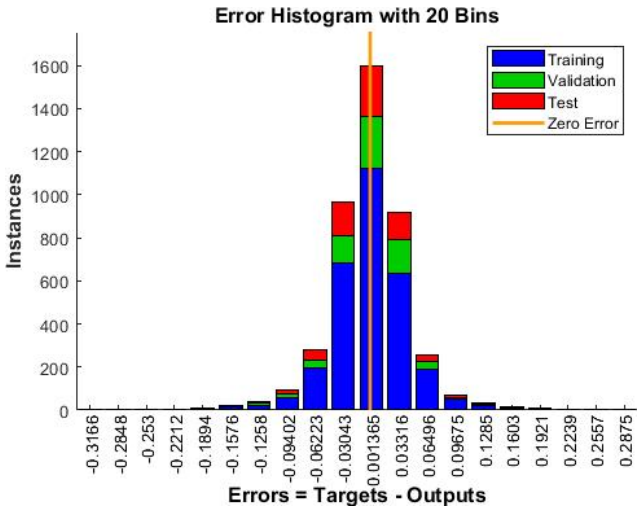

Fig. 5 Histogram error in the case of 2 hidden layers

0.001365. This implies that by increasing the complexity of the model, achieved by adding more neurons and hidden layers, the model's performance has been enhanced.

The discernible distinctions in accuracy are apparent in Figs. 6 and 7 presented below, where the performance of the two-layer configuration surpasses that of the single-layer arrangement. In the first case, the accuracy for training data stands at 0.99512. In contrast to this, the second case exhibits superior accuracy with a value of 0.99892. This pattern is similarly reflected in the validation data, where the initial scenario registers an accuracy of 0.99408, while the second case excels with a higher accuracy score of 0.99886. The trend continues in case the testing data, with the first case recording an accuracy of 0.9949, while the second case excels further with an accuracy of 0.9989.

Consequently, when utilizing a neural network architecture featuring two hidden layers, we observe enhanced performance in comparison to the one-layer counterpart.

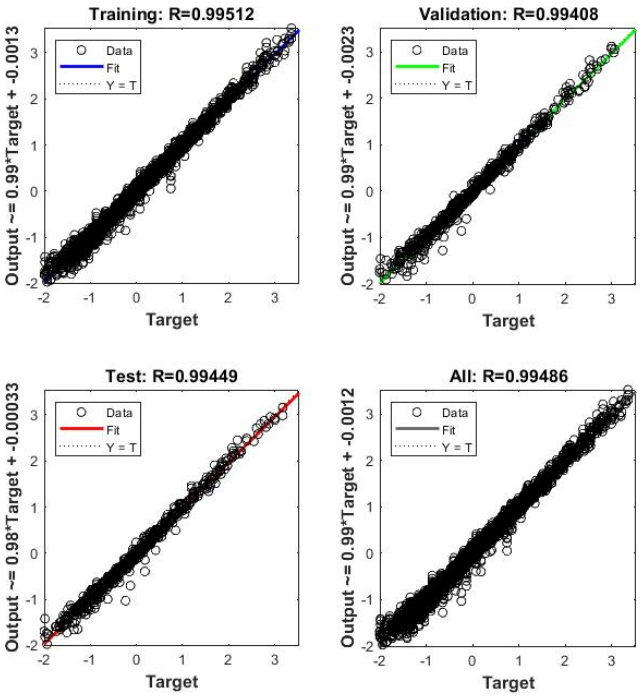

Fig. 6 Training, testing and validation data in the case of 1 hidden layer

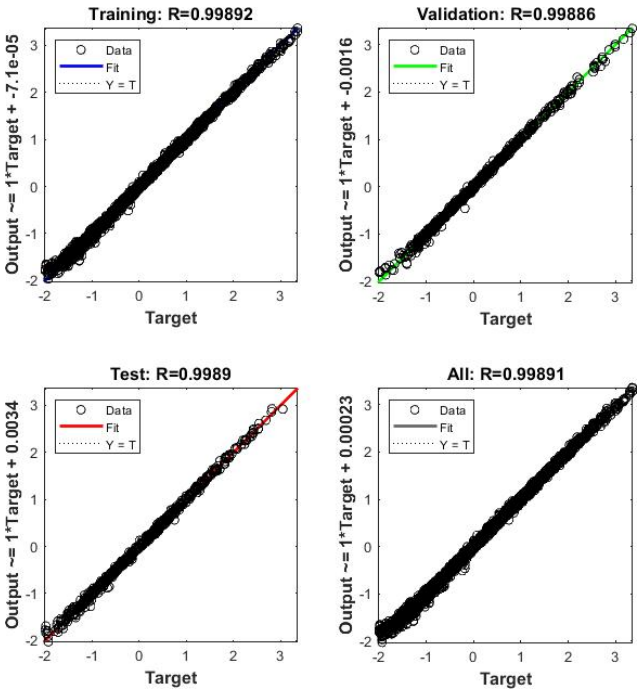

Fig. 7 Training, testing and validation data in the case of 2 hidden layers

This improvement is particularly evident regarding the validation results, achieved within a reduced number of training epochs. In case of 2 hidden layers the learning process was faster (Figs. 8 and 9).

3.3 Comparison of the models

The base of the comparison is the analysis of the error. Figs. 10 and 11 present the calculated and the estimated values of the effective diameter and the distribution of the

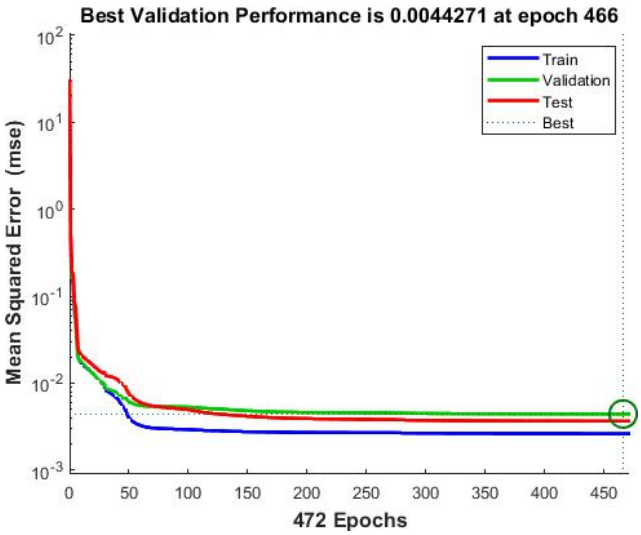

Fig. 8 Validation performance in the case of 1 hidden layer (*a*1)

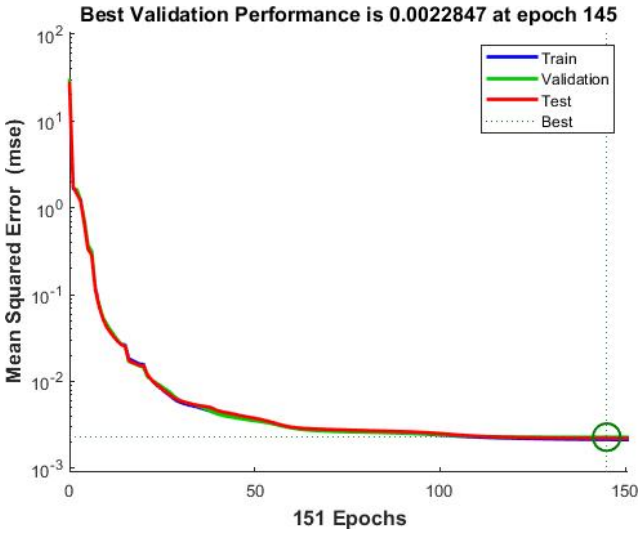

Fig. 9 Validation performance in the case of 2 hidden layers (*a*2)

differences. Only the data of D_{eff_1} is presented, given that the results of D_{eff_2} show similar tendencies.

In case of the *r*1 model, as shown in Fig. 10 (a) and (b), the estimated values have remarkable error. The point clouds follow the ideal line, but the area is too wide. Moreover, some negative values are also included. The inaccuracy of the regression can be seen in the histogram of the differences. The range of the differences is 3.899 mm, the histogram is flat, and the standard deviation is 0.562 mm. Four ramifications can be seen at the top region, which are connected to the four different *D*s.

The *r*2 regression model shows better accuracy (Fig. 10 (c) and (d)). The point cloud is narrower, and the histogram has higher peak. The range is little bit smaller (3.118 mm), and the standard deviation is 0.329 mm. The larger deviation can be observed under 6 mm.

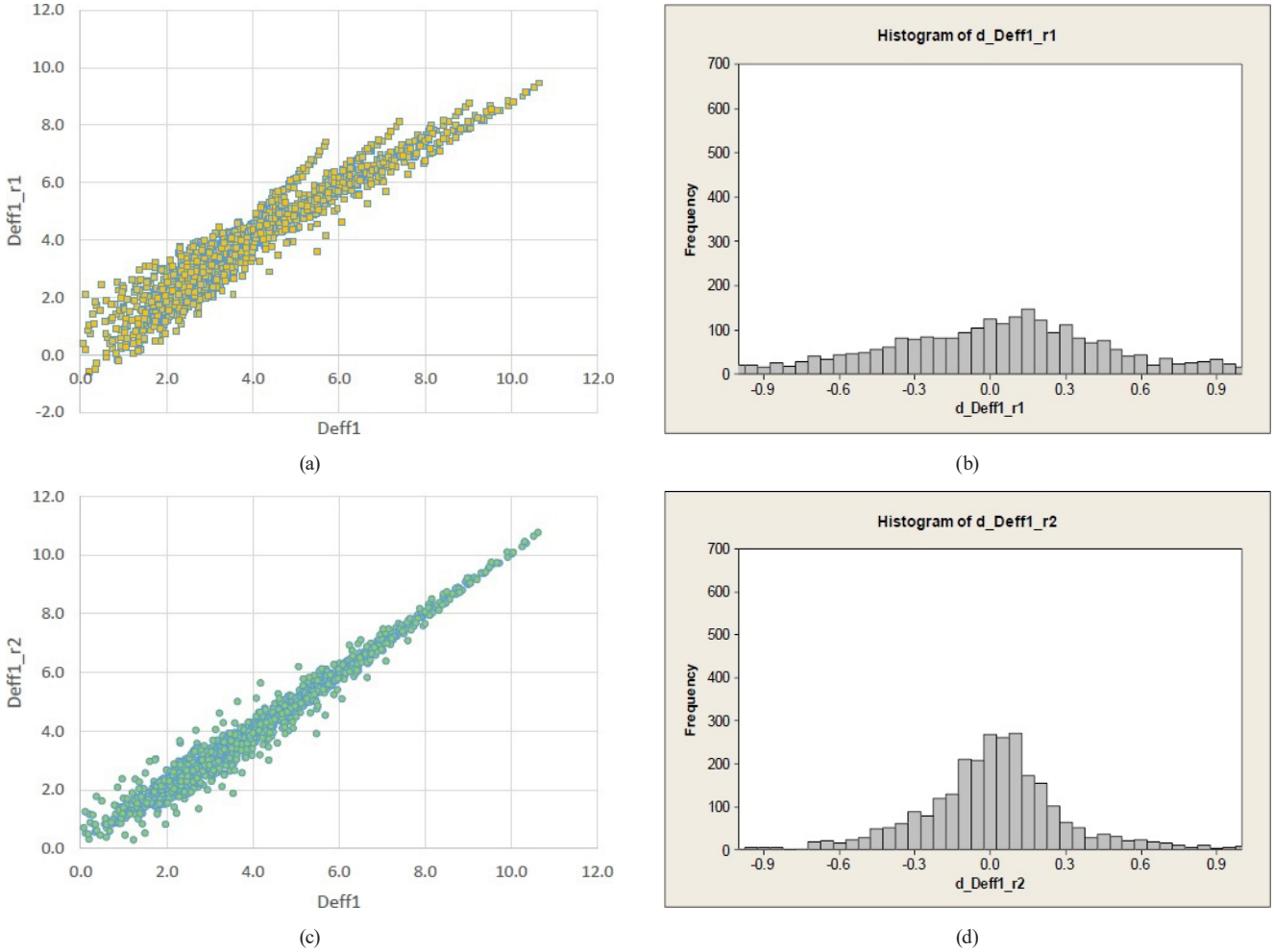

Fig. 10 The calculated and the estimated values of the effective diameter and the distribution of the error of regression models: (a) *r*1; (b) *r*1; (c) *r*2; (d) *r*2

The ANN models show better performances. The *a*1 model (Fig. 11 (a) and (b)) has narrow point cloud, but some outlier data can be observed. In case of small working diameter, the error is larger, a small curve can be seen in the diagram. The histogram of the error shows normal distribution, the range is 2.601 mm and the standard deviation is 0.194 mm.

The *a*2 neural model shows the best accuracy. The point cloud in Fig. 11 (c) is very thin, but under 1 mm a pattern can be observed, similar to the case of the *a*1 model. The histogram is narrow and tall, the range is 1.113 mm and the standard deviation is 0.080 mm only. The *a*2 ANN model results the smallest error within all the cases.

The improving accuracy of the different methods is shown in the previously presented diagrams, but the statistic parameters can describe more precisely (Table 4 and Fig. 12).

The range of the error values indicates the inaccuracy of the methods, but this is only a rough characterization. The standard deviation can describe the nature of the histogram, the distribution of the values of the error. In case of the presented models, the range and the standard deviation had smaller and smaller values.

The R^2 is 91.9% in case of the *r*1 model, which is generally a good regression, but as the previous analysis has shown, the local error can be large in some cases. In case of ANN model, the R^2 are 99.0% and 99.8%, which signifies a very good regression.

The standard deviation, the RMSE and the MAPE changed parallel (Fig. 12). The relative values of the standard deviation, the RMSE and the MAPE changed similar, in case of the *r*2 the values are 58% – 58% – 59%; in case of the a1: 35% – 37% – 42% and in case of the *a*2: 14% – 14% and 19% comparing to the *r*1 model. Although these parameters measure the different aspects of the deviation, their values changed parallelly.

4 Conclusions

In case of ball-end milling of free form surfaces, the working diameter changes parallelly with the A_{N2}. The working diameter depends on the D, the a_p, the A_{N2} and the A_f.

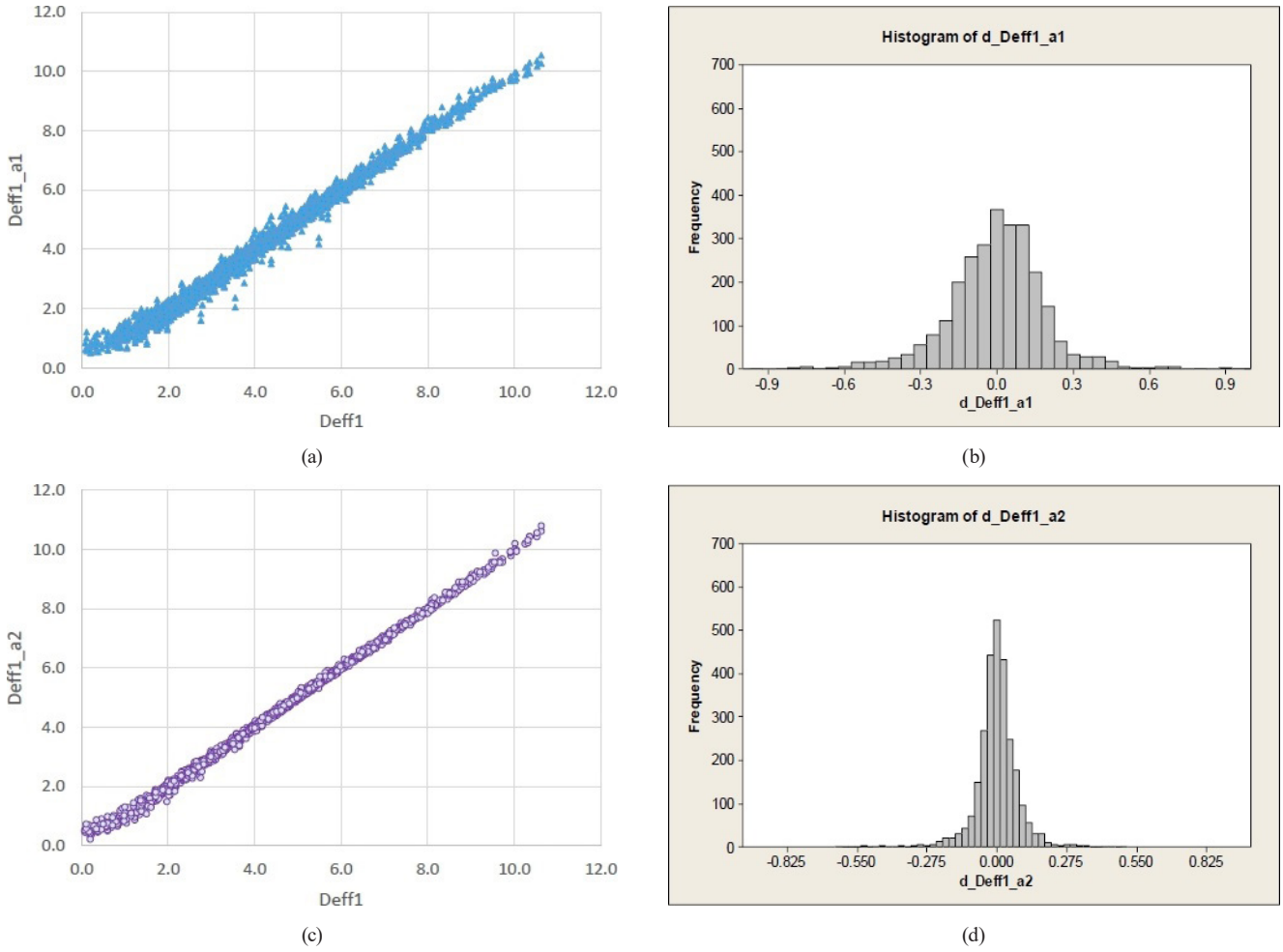

Fig. 11 The calculated and the estimated values of the effective diameter and the distribution of the error of ANN models: (a) *a*1; (b) *a*1; (c) *a*2; (d) *a*2

Table 4 The values of the statistical parameters of the differences

Model	*r*1	*r*2	*a*1	*a*2
Range	3.899	3.118	2.601	1.113
Standard deviation	0.562	0.329	0.194	0.080
R^2	0.919	0.972	0.990	0.998
RMSE	0.562	0.329	0.194	0.080
MAPE	0.194	0.114	0.082	0.038

In this article the geometric model, two types of regression models and two ANN models were compared based on the statistical parameters of the error values. The base of the investigation was a set of data, which contains 2704 variations of input parameters. The performances of the models were compared by the range of the error, the standard deviation, the R^2, the RMSE and the MAPE.

The results can be summarized as follows:

1. To introduce the relative A_f, due to the inherent periodic behavior of the geometric model, the number of input parameters can be reduced. Utilizing the relative A_f in the regression equation for the working diameter proved to be advantageous. To establish an appropriate regression model, the multiplication of the first, third, and fifth powers of the A_{N2} and the relative A_f is essential.
2. A separated regression model based on the D yields improved accuracy, the coefficients can be computed as a function of the D. This approach facilitates the creation of a unified regression model, streamlining the modelling process and ensuring consistency across different Ds.
3. The integration of the ANNs into prediction models seeks to harness their learning capabilities, constructing precise and resilient models for making informed predictions about the working diameter in end ball milling. This adaptation ensured accuracy and reliability in real-world milling scenarios by leveraging relevant cutting parameters. The ANN based model showed the best performances. The standard deviation, the RMSE and MAPE parameters, although these parameters measure the different aspects of the deviation, their values changed parallel and to the same extent.

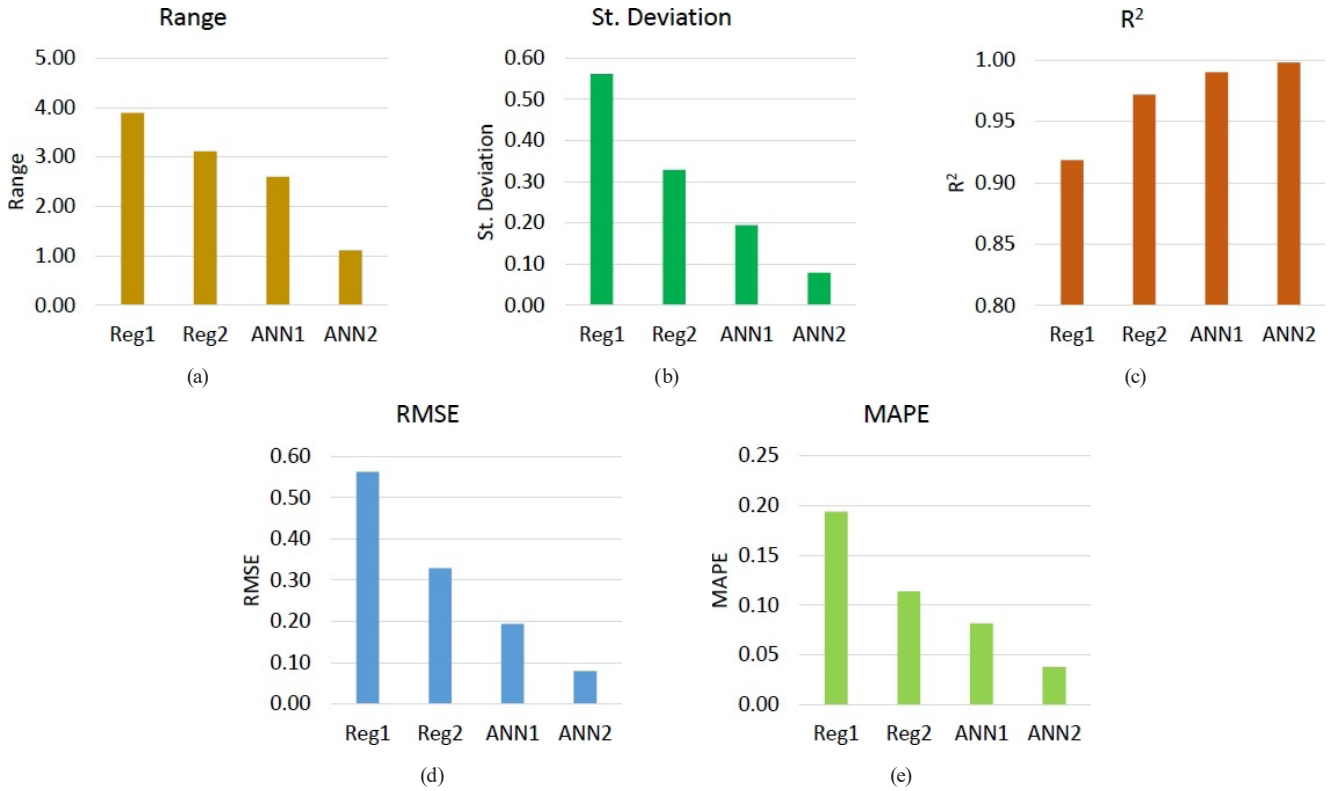

Fig. 12 Values of the differences: (a) the range; (b) the standard deviation; (c) the R^2; (d) the RMSE; (e) the MAPE

The working diameter of the ball-end milling cutter can be used during the adaptive modification of the cutting parameters in order to keep the constant value of the cutting speed and the feed. Taking into account the A_{N2} at the current tool position based on the CAD model and the milling direction, the spindle speed for a constant cutting speed can be calculated, thus improving machining conditions and surface quality. During the tool path planning of finishing milling of a free form surface the current value of the working diameter can be used, in order to minimize the changing of it. These applications require a fast and accurate calculation method.

References

[1] Lotfi, S., Rami, B., Maher, B., Gilles, D., Wassila, B. "Cutter-workpiece engagement calculation in 3-axis ball-end milling considering cutter runout", Journal of Manufacturing Processes, 41, pp. 74–82, 2019. https://doi.org/10.1016/j.jmapro.2019.03.025

[2] Forootan, M., Akbari, J., Ghorbani, M. "A new geometric approach for real-time cutting force simulation in 3-axis ball-end milling compatible with graphical game engines", The International Journal of Advanced Manufacturing Technology, 128(9), pp. 4003–4022, 2023. https://doi.org/10.1007/s00170-023-12025-5

[3] Feng, H.-Y., Su, N. "A Mechanistic Cutting Force Model for 3D Ball-end Milling", Journal of Manufacturing Science and Engineering, 123(1), pp. 23–29, 2001. https://doi.org/10.1115/1.1334864

[4] Ko, J. H., Cho, D.-W. "3D Ball-End Milling Force Model Using Instantaneous Cutting Force Coefficients", Journal of Manufacturing Science and Engineering, 127(1), pp. 1–12, 2005. https://doi.org/10.1115/1.1826077

[5] Ghorbani, M., Movahhedy, M. R. "An analytical model for cutter-workpiece engagement calculation in ball-end finish milling of doubly curved surfaces", The International Journal of Advanced Manufacturing Technology, 102(5), pp. 1635–1657, 2019. https://doi.org/10.1007/s00170-018-3188-y

[6] Wei, Z. C., Wang, M. J., Zhu, J. N., Gu, L. Y. "Cutting force prediction in ball-end milling of sculptured surface with Z-level contouring tool path", International Journal of Machine Tools and Manufacture, 51(5), pp. 428–432, 2011. https://doi.org/10.1016/j.ijmachtools.2011.01.011

[7] Wei, Z. C., Wang, M. J., Cai, Y. J., Wang, S. F. "Prediction of cutting force in ball-end milling of sculptured surface using improved Z-map", The International Journal of Advanced Manufacturing Technology, 68(5), pp. 1167–1177, 2013. https://doi.org/10.1007/s00170-013-4909-x

[8] Nishida, I., Okumura, R.., Sato, R., Shirase, K. "Cutting Force Simulation in Minute Time Resolution for Ball-end Milling Under Various Tool Posture", Journal of Manufacturing Science and Engineering, 140(2), 021009, 2018.
https://doi.org/10.1115/1.4038499

[9] Mikó, B., Zentay, P. "A geometric approach of working tool diameter in 3-axis ball-end milling", The International Journal of Advanced Manufacturing Technology, 104(1), pp. 1497–1507, 2019.
https://doi.org/10.1007/s00170-019-03968-9

[10] Mgherony, A., Mikó, B. "Simulation of the Working Diameter in 3-Axis Ball-end Milling of Free Form Surface", Tehnički Vjesnik, 29(4), pp. 1164–1170, 2022.
https://doi.org/10.17559/TV-20210719181212

[11] Cheng, M., Jiao, L., Yan, P., Qiu, T., Wang, X., Zhang, B. "Prediction of surface residual stress in end milling with Gaussian process regression", Measurement, 178, 109333, 2021.
https://doi.org/10.1016/j.measurement.2021.109333

[12] Lu, J., Zhang, Z., Yuan, X., Ma, J., Hu, S., Xue, B., Liao, X. "Effect of machining parameters on surface roughness for compacted graphite cast iron by analyzing covariance function of Gaussian process regression", Measurement, 157, 107578, 2020.
https://doi.org/10.1016/j.measurement.2020.107578

[13] Xu, J., Xu, L., Geng, Z., Sun, Y., Tang, K. "3D surface topography simulation and experiments for ball-end NC milling considering dynamic feedrate", CIRP Journal of Manufacturing Science and Technology, 31, pp. 210–223, 2020.
https://doi.org/10.1016/j.cirpj.2020.05.011

[14] Denkena, B., Böß, V., Nespor, D., Gilge, P., Hohenstein, S., Seume, J. "Prediction of the 3D Surface Topography after Ball End Milling and its Influence on Aerodynamics", Procedia CIRP, 31, pp. 221–227, 2015.
https://doi.org/10.1016/j.procir.2015.03.049

[15] Wojciechowski, S. "The estimation of cutting forces and specific force coefficients during finishing ball end milling of inclined surfaces", International Journal of Machine Tools and Manufacture, 89, pp. 110–123, 2015.
https://doi.org/10.1016/j.ijmachtools.2014.10.006

[16] Santhakumar, J., Iqbal, U. M. "Role of trochoidal machining process parameter and chip morphology studies during end milling of AISI D3 steel", Journal of Intelligent Manufacturing, 32(3), pp. 649–665, 2021.
https://doi.org/10.1007/s10845-019-01517-5

[17] Lin, Y.-C., Wu, K.-D., Shih, W.-C., Hsu, P.-K., Hung, J.-P. "Prediction of Surface Roughness Based on Cutting Parameters and Machining Vibration in End Milling Using Regression Method and Artificial Neural Network", Applied Sciences, 10(11), 3941, 2020.
https://doi.org/10.3390/app10113941

[18] Xie, J., Zhao, P., Hu, P., Yin, Y., Zhou, H., Chen, J., Yang, J. "Multi-objective feed rate optimization of three-axis rough milling based on artificial neural network", The International Journal of Advanced Manufacturing Technology, 114(5), pp. 1323–1339, 2021.
https://doi.org/10.1007/s00170-021-06902-0

[19] Kannadasan, K., Edla, D. R., Yadav, M. H., Bablani, A. "Intelligent-ANFIS Model for Predicting Measurement of Surface Roughness and Geometric Tolerances in Three-Axis CNC Milling", IEEE Transactions on Instrumentation and Measurement, 69(10), pp. 7683–7694, 2020.
https://doi.org/10.1109/TIM.2020.2980599

[20] Shankar, S., Mohanraj, T., Rajasekar, R. "Prediction of cutting tool wear during milling process using artificial intelligence techniques", International Journal of Computer Integrated Manufacturing, 32(2), pp. 174–182, 2019.
https://doi.org/10.1080/0951192X.2018.1550681

[21] Varga, J., Ižol, P., Vrabeľ, M., Kaščák, Ľ., Drbúl, M., Brindza, J. "Surface Quality Evaluation in the Milling Process Using a Ball Nose End Mill", Applied Sciences, 13(18), 10328, 2023.
https://doi.org/10.3390/app131810328

[22] Globocki Lakić, G., Sredanović, B., Jotić, G., Gotovac, S. "Komparativna analiza strategija glodanja površina složene geometrije" (A comparative analysis of milling strategies of complex geometry surfaces), FME Transactions, 50(4), pp. 623–634, 2022. (in Croatian)
https://doi.org/10.5937/fme2204623G

[23] Minitab Inc. "MiniTab, (v14)", [computer program] Available at: http://www.minitab.com [Accessed: 22 October 2024]

[24] Microsoft "Excel, (2017)", [computer program] Available at: http://www.microsoft.com [Accessed: 22 October 2024]

[25] The MathWorks, Inc. "MATLAB, (R2024b)", [computer program] Available at: http://www.ch.mathworks.com [Accessed: 22 October 2024]

[26] Saha, N., Swetapadma, A., Mondal, M. "A Brief Review on Artificial Neural Network: Network Structures and Applications", In: 2023 9th International Conference on Advanced Computing and Communication Systems (ICACCS), Coimbatore, India, 2023, pp. 1974–1979. ISBN 979-8-3503-9738-3
https://doi.org/10.1109/ICACCS57279.2023.10112753

[27] Solís-Pérez, J. E., Hernández, J. A., Parrales, A., Gómez-Aguilar, J. F., Huicochea, A. "Artificial neural networks with conformable transfer function for improving the performance in thermal and environmental processes", Neural Networks, 152, pp. 44–56, 2022.
https://doi.org/10.1016/j.neunet.2022.04.016

[28] The MathWorks, Inc. "MATLAB Neural Network Toolbox", [computer program] Available at: http://www.ch.mathworks.com [Accessed: 22 October 2024]